Self-Starting 6.5-fs Pulses from a Ti:Sapphire Laser Using a Semiconductor Saturable Absorber and Double-Chirped Mirrors

Dirk H. Sutter, Isabella D. Jung, Franz X. Kärtner, Nicolai Matuschek, François Morier-Genoud, V. Scheuer, M. Tilsch, T. Tschudi, and Ursula Keller, *Member, IEEE*

***Abstract*— We demonstrate self-starting 6.5-fs pulses from a Kerr-lens-mode-locked Ti:sapphire laser with an average output power of 200 mW at a pulse repetition rate of 86 MHz. We have achieved a mode-locking buildup time of only 60 μs, using a broad-band semiconductor saturable absorber mirror to initiate the pulse formation. The dispersion has been compensated with a prism pair in combination with improved double-chirped mirrors. The prism pair allows for the flexible adjustment of both the duration and the center wavelength of the pulse. The double-chirped mirrors show a high reflectivity better than 99.8% over the full bandwidth of 300 nm and a controlled group delay over more than 250 nm. The choice of a proper output coupler turns out to be critical for ultrashort pulse generation directly from the laser.**

***Index Terms*— Chirped mirrors, dispersion control, femtosecond phenomena, laser resonators, pulsed lasers, semiconductor saturable absorbers, solid lasers, ultrafast optics.**

I. Introduction

RAPID PROGRESS in ultrashort pulse generation with Ti:sapphire lasers began with the first demonstration of Kerr-lens-mode-locking (KLM) [1]. In 1994, sub-10-fs pulses were generated directly from a laser for the first time [2]. Novel dispersion compensation techniques have led to pulses as short as 7.5 fs [3]. The currently shortest Ti:sapphire laser pulses have a duration of 6.5 fs, and are obtained from a reliable, self-starting oscillator [4]. This latest result will be discussed in more detail in this paper.

The continuing improvements in ultrafast laser technology have led to many new and fascinating applications in physics, engineering, chemistry, biology, and medicine. While these applications are the major driving force for the development of novel laser sources, the specific requirements are rather diverse. It is obvious that all applications benefit from a reliable, stable and "hands-off" ultrafast laser. Our latest developments of broad-band semiconductor saturable absorber mirrors (SESAM's) [5], [6] and controlled dispersion compensation with double-chirped mirrors (DCM's) [7], [8] are the key features for an ultrafast laser technology which approaches the requirements for "hands-off" operation. We give a comprehensive description of the generation of 6.5-fs pulses with an improved mode-locking buildup time of 60 μs. The average output power is 200 mW, at a pulse repetition rate of 86 MHz. Without KLM, the limited modulation depth of the SESAM supports sub-20-fs pulses over the full cavity stability regime. We only obtain self-starting 6.5-fs pulses when we combine the SESAM with KLM. The cavity stability adjustments are less critical when SESAM's are used compared to KLM alone.

To date, shorter pulses of $\approx$4.5 fs have only been generated by external pulse compression of cavity-dumped Ti:sapphire laser pulses at pulse repetition rates up to a megahertz [9], [10], and by compression of amplified high energy pulses at pulse repetition rates in the kilohertz regime [11], [12]. The latter approach resulted in 4.5-fs pulses with a pulse energy up to 70 μJ [12] and, more recently, in 5-fs pulses with an energy of 0.5 mJ [13]. These large peak powers will be extremely interesting for high harmonic generation [14], [15], particularly for coherent "water window" X-rays [16], [17]. The water window lies between 2.2 and 4.4. nm, where water is transparent, but carbon strongly absorbs. This makes it an ideal wavelength range for the microscopy of living cells.

In contrast, ultrashort pulses like the ones described here, i.e., at lower pulse energies in the nanojoule regime and at the repetition rate of the oscillator, are very interesting for "low-excitation-level" laser spectroscopy. The higher pulse repetition rates substantially improve the signal-to-noise ratio (SNR) of such measurements. A broad coherent spectrum of ultrashort pulses at high repetition rates can contribute to a wide range of applications in information processing and communications, such as high-density wavelength-division multiplexing [18], interconnects and networking [19], as well as optical coherence tomography [20]. Ultrashort pulses with durations well below the dephasing time in atomic systems and solid state media are needed for the investigation of coherent dynamics. They might become interesting for quantum computing as well [21].

The ultimate limit in laser pulse duration can be estimated from the gain bandwidth of the laser medium, not considering additional spectral broadening of the pulses due to self-phase modulation (SPM). Fourier transformation of the gain spectrum of Ti:sapphire yields an expected minimum pulse duration of about 5 fs. All the laser optics, mirrors, output

Manuscript received October 10, 1997; revised February 9, 1998. This work was supported by the Swiss National Science Fund.

D. H. Sutter, I. D. Jung, F. X. Kärtner, N. Matuschek, F. Morier-Genoud, and U. Keller are with the Institute of Quantum Electronics, Swiss Federal Institute of Technology (ETH), ETH-Hönggerberg HPT, CH-8093 Zürich, Switzerland.

V. Scheuer, M. Tilsch, and T. Tschudi are with the Institute for Applied Physics, Technical University Darmstadt, D-64289 Darmstadt, Germany.

Publisher Item Identifier S 1077-260X(98)03765-4.

couplers, the mode-locking mechanism (e.g., KLM) and the self-starting mechanism (e.g., a SESAM) have to be designed for optimum performance over this wavelength range. The main issue in the development of sub-10-fs lasers is the proper control of the wavelength-dependent cavity round-trip time, or group delay. In order to balance the SPM effects, the group delay dispersion *(GDD)* of the laser material needs to be slightly overcompensated for soliton pulse formation [22] and soliton mode-locking [23]–[25].

The history of KLM Ti:sapphire lasers illustrates the limitations due to intracavity dispersion. The standard compensation technique used in sub-100-fs lasers involves prism-pairs [26], which simultaneously allow for wavelength tunability and continuous adjustments of the pulse width. Unfortunately, the different higher orders of prism dispersion cannot be controlled independently [27]–[30]. The first Ti:sapphire laser that generated sub-10-fs pulses [2] avoided higher order dispersion by using silver mirrors and a thin laser crystal, and by lasing at 850 nm, where the third-order dispersion of the fused quartz prism pair vanishes. In this way, pulses as short as 8.5 fs were achieved, with an output power of up to 30 mW. The laser was not self-starting. The next major progress produced pulses as short as 7.5-fs duration, with a higher average output power of a few hundred milliwatts [3], [31]. The main reason for this advance was the development of chirped mirrors [32], [33]. In a chirped mirror, the longer wavelengths penetrate more deeply into the mirror structure than do the shorter wavelengths. This leads to a negative GDD that compensates for the positive GDD of the laser crystal. Using chirped mirrors, negative GDD can thus be obtained with hardly any additional higher order dispersion. Though dispersion compensation with chirped mirrors alone supports compact oscillators, the fixed cavity dispersion limits the tunability of the pulse parameters [3], [32], [34]. Without using prisms, we can only adjust the negative dispersion by a fixed, discrete amount per reflection.

Continuous adjustment of the intracavity GDD using prism pairs is necessary for optimized performance. Therefore, we prefer to use the prism pair in combination with chirped mirrors, that compensate for the higher order dispersion of the prism pair. We have developed new analytic design guidelines for chirped mirrors by chirping both the Bragg wavelength and the thickness of the high-index layer [7], [8]. These "double-chirped mirrors" (DCM's) show an extended high reflectivity range of more than 300 nm, resulting in 6.5-fs pulses directly from the laser. The intracavity pulse was $\approx$9 fs and, thus, considerably longer than the output pulse. The 6.5-fs pulses have been obtained due to the special transmission characteristic of the output coupler, which lifts the wings of the spectrum.

Another key-issue for reliable operation of sub-10-fs lasers is the mode-locking starting mechanism, obtained with a broad-band SESAM. A KLM-laser without a SESAM usually has to be operated near one limit of the resonator stability regime. Furthermore, the pulse formation process needs to be started by a brief physical perturbation, such as a shaking mirror inside an external coupled resonator. The startup behavior of the laser critically depends on the modulation depth and the saturation intensity of the absorber. Both parameters have been improved in a new SESAM design which reduces the mode-locking buildup time from 3 ms [4] to 60 μs. This paper gives insight in the properties of the broad-band SESAM, the DCM's, and the output coupler which supported self-starting 6.5-fs pulses from the Ti:sapphire laser. The laser is characterized in terms of mode-locking buildup time, spectrum, and interferometric autocorrelation (IAC).

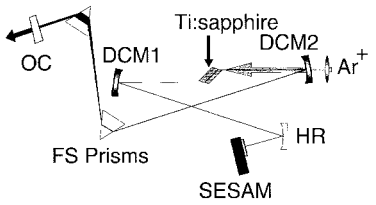

Fig. 1. The Ti:sapphire laser cavity, which consists of two double-chirped mirrors (DCM1, DCM2) and a fused-silica (FS) prism pair for compensation of second and higher order dispersion. A standard HR focuses onto the SESAM, which self-starts the mode-locking process. The Ti:sapphire crystal is 2.3 mm long and has a doping of 0.25% wt.

II. The Laser Setup

A. Cavity Design

The experimental setup is shown in Fig. 1. The Ti:sapphire crystal plate, with a thickness of 2.3 mm and a titanium doping of 0.25% wt., is inserted at Brewster's angle. The laser is pumped by all lines of an argon ion laser with a typical pump power of 6-W and a focused beam diameter of 45 μm (tangential) and 25 μm (sagittal). All mirrors have a 10 cm radius of curvature and the flat output coupler (OC) shows an average transmission of 3%. The total cavity length of approximately 1.75 m corresponds to a pulse repetition rate of 86 MHz. The linear resonator includes a fused quartz prism pair at an apex-to-apex distance of 40 cm. The DCM's compensate for the higher order dispersion of the prism pair. The total cavity GDD can be varied by changing the insertion of the prisms into the beam. For self-starting of the KLM process, we focused the laser mode to a spot diameter of about 20 μm onto a broad-band SESAM at one end of the linear cavity. This incident spot size on the SESAM determines the saturation power of the absorber.

B. Broad-Band SESAM for Self-Starting Mode-Locking

Semiconductor saturable absorbers have been successfully used to passively mode-lock laser diodes [35], [36]. In 1992, for the first time, an intracavity SESAM continuous-wave (CW) mode-locked a solid-state laser with a longer upper state lifetime (i.e., greater than about one μs) without Q-switching instabilities [37]. Since then, many different solid-state lasers have been successfully CW mode-locked with various intracavity SESAM's. A recent review is given in [38] and in a book chapter [39]. To date, the shortest pulses which use only SESAM's for mode-locking without the assistance of KLM are 13 fs in duration [25]. Presently, we do not have saturable absorbers with a sufficiently large modulation depth over a bandwidth broad enough to directly mode-lock

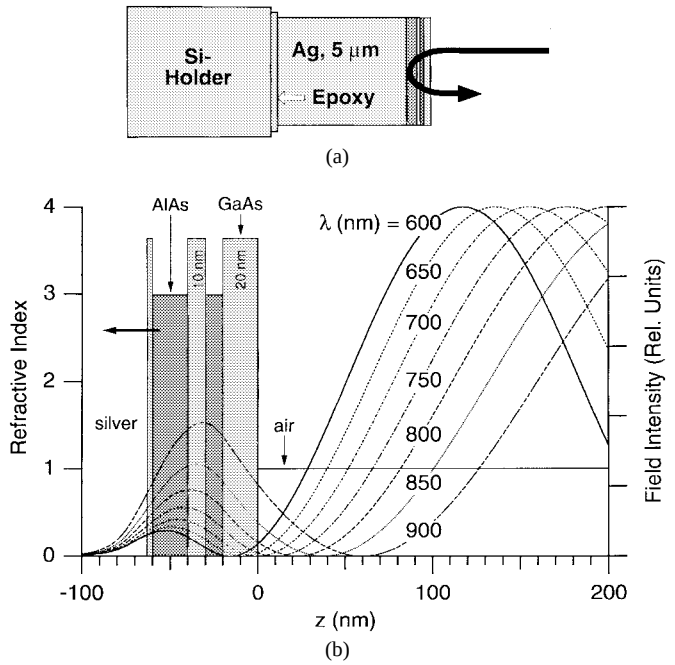

Fig. 2. (a) The SESAM structure, which consists of two GaAs quantum wells (QW's) of 20 and 10 nm thickness, separated by a barrier of 10-nm AlAs. Between the thinner QW and the GaAs cap layer, there is another 20-nm-thick AlAs layer. The evaporated bottom silver mirror is glued to a silicon holder with silver epoxy. (b) The refractive indexes (left axis) and the standing wave pattern (right axis), calculated for low intensity light at wavelengths l from 600 to 900 nm.

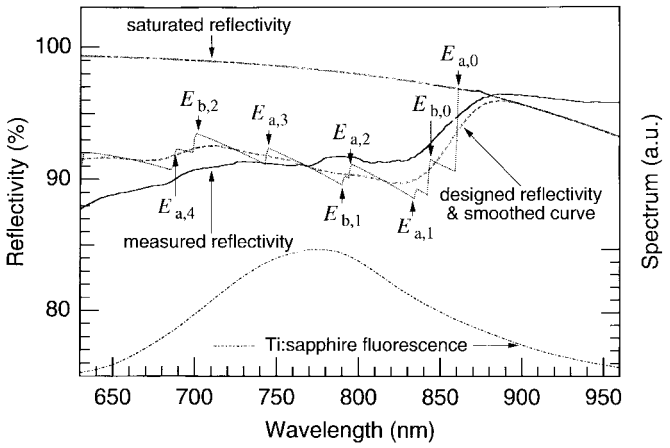

Fig. 3. Measured and calculated low intensity reflectivity of the SESAM, plotted over the whole fluorescence spectrum range of Ti:sapphire. The steps, which are due to transitions from the heavy hole bands of the two QW's (a) 20 nm and (b) 10 nm, are indicated in the design. The smoothed curve was obtained from the designed curve by applying a 40-nm-wide smoothing filter. The reflectivity for full saturation was calculated by setting the GaAs absorption to zero.

sub-10-fs lasers. However, we have demonstrated broad-band saturable absorbers that are strong enough to start KLM pulses in the sub-10-fs regime, with sub-100-μs mode-locking buildup times [5], [6].

The SESAM structure used in this work is shown in Fig. 2(a). The saturable absorber consists of two GaAs quantum wells located inside an antiresonant Fabry–Perot. Antiresonance is important in order to minimize wavelength dependent reflections of the Fabry–Perot structure, and to adjust the saturation energy. The Fabry–Perot structure is formed by a lower silver mirror and the Fresnel reflection at the semiconductor/air interface. The much lower partial reflections at the AlAs–GaAs interface are negligible compared to the top and bottom mirror reflection. The total thickness d of the Fabry–Perot structure is adjusted for antiresonance for a wavelength $\approx$700 nm with two transparent AlAs spacer layers between the GaAs absorbers. The antiresonance condition is fulfilled for a Fabry–Perot round-trip phase φ_{rt} of $(2m+1)\pi$, where m is an integer. The round-trip phase is then given by the phase shift at the silver mirror φ_b, a phase shift $\varphi_t = 0$ at the semiconductor/air interface, and a material phase shift $2k\overline{n}d$, resulting in $\varphi_{rt} = 2k\overline{n}d + \varphi_b = 3\pi$, where $\overline{n}$ is the average refractive index of the GaAs and AlAs layers. The penetration depth into the silver mirror is taken into account with the phase shift φ_b.

The exact position and thickness of the GaAs absorber layer is numerically optimized using a transfer matrix calculus, with complex refractive indices that include absorption. The absorption of thin layers of GaAs embedded between AlAs barriers differs from the bulk value due to quantum confinement. In a simplified model for the quantum well, we replace the bulk absorption with a step function that changes at the specific energies of the transition between the heavy hole and the conduction band. At each transition energy the absorption simply takes the corresponding bulk value, and then remains constant with decreasing wavelength until the next transition energy is reached. The position and thickness of the GaAs absorber layers as well as the exact wavelength for antiresonance are chosen such that the standing wave profile partially compensates for the wavelength-dependent absorption in GaAs. This takes into account that an absorber layer located in a node of the standing wave at a given wavelength has reduced absorption at that wavelength.

Fig. 2(b) shows the calculated standing wave pattern for various wavelengths from 600 to 900 nm. The 20-nm-thick GaAs quantum well in the front, with an absorption edge at 860 nm, is located at the maximum of the standing waves for the longer wavelength. The 10-nm-thin quantum well in the back with an absorption edge at 840 nm does not introduce absorption for the long wavelengths and is located in the maximum of the standing waves for the short wavelengths. The third GaAs layer is too thin to significantly add to the absorption. Fig. 3 shows the resulting calculated and measured low-intensity reflectivity, together with the fluorescence of Ti:sapphire. The reflectivity step around 860 nm corresponds to the band edge of the thick absorber layer. The confinement energies for the quantum wells were calculated with standard band parameters for the effective masses and the energy gaps [40]. Absorption edges due to the transitions from the light hole or split-off band have not been considered in the simplified absorption model. At room temperature, the discrete edges due to the transitions between the heavy holes and the conduction band are washed out. This can be simulated with a smoothing filter (Fig. 3). When fully saturated, the reflectivity should be nearly flat, to avoid any additional intracavity filtering. However, intervalley scattering will limit the saturation for wavelengths shorter than 715 nm [6], [41].

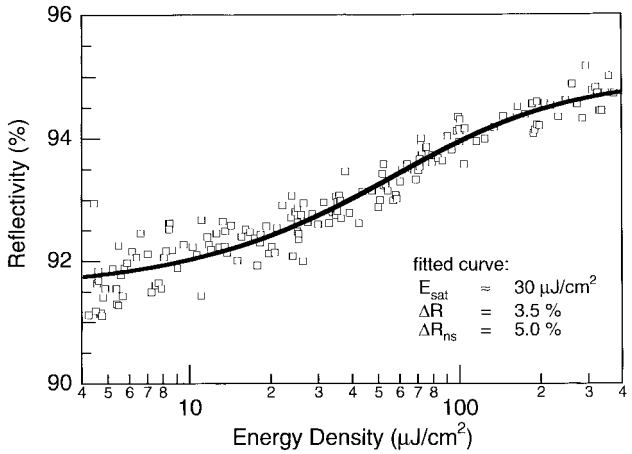

Fig. 4. Reflectivity of the SESAM as a function of incident laser fluence, measured with 100-fs pulses. The saturation of the SESAM absorption occurs at a fluence of about 30 μJ/cm^2. The modulation depth, i.e., the amount of saturable absorption, is 3.5%. The residual nonsaturable losses are 5%. Similar curves have also been measured with shorter pulses, but those are of less relevance for the pulse buildup.

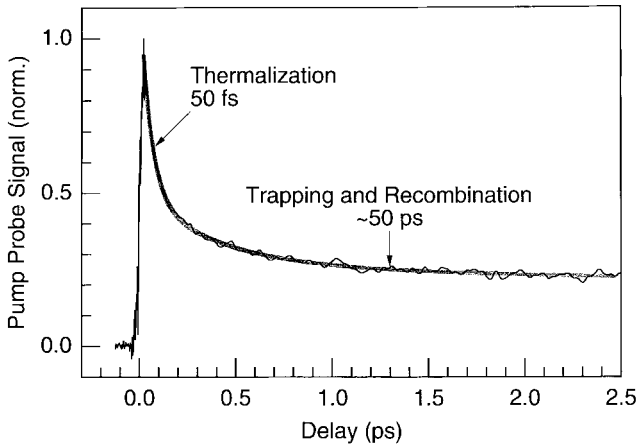

Fig. 5. Pump probe transients measured with 20-fs pulses. The response shows a short decay time of 50 fs due to intraband thermalization of the excited carriers. The long recovery time, on the order of 50 ps, is due to carrier trapping and recombination.

The fabrication process consists of the following main steps and is discussed in more detail in [5]: First, the absorber layer is grown on a GaAs substrate. Then a silver layer is deposited on top of the absorber. A silicon wafer is glued to this silver reflector. Finally, the GaAs substrate is etched away using bromine and HCl. Thus, in the final structure the absorber sits on a silver mirror fixed to a silicon wafer holder. SESAM's with the structure described above were also used in earlier experiments [6]. However, the improved SESAM shows an extended wavelength range of constant linear absorption, and the standard temperature MBE growth of the absorber structure leads to a larger modulation depth and a longer absorber recovery time. A modulation depth of $\Delta R = 3.5\%$ has been measured using 100-fs pulses (Fig. 4) compared with 1% in [4]. The measured saturation fluence decreased to a third from $E_{\rm sat} = 100$ mJ/cm^2 [4] to $E_{\rm sat} = 30$ mJ/cm^2. The measured impulse response (Fig. 5), using 20-fs pulses, exhibits a fast decay with a 50-fs time constant followed by a recovery time

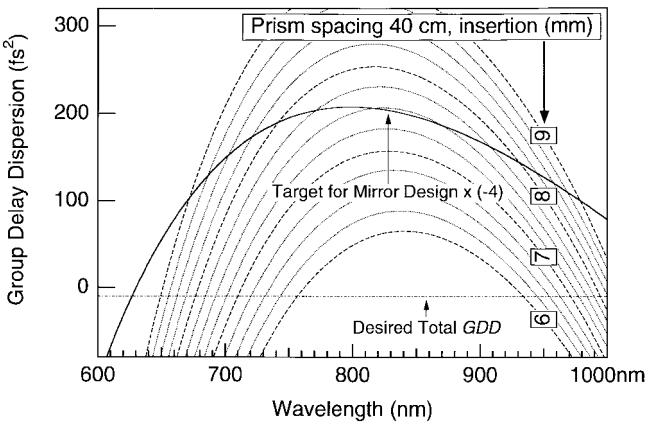

Fig. 6. GDD for a round-trip through a 2.3-mm Ti:sapphire crystal and a FS prism pair, calculated for a tip-to-tip prism separation of 40 cm and for different prism insertions from 6 to 9 mm in steps of 250 μm. The target function of the design for the double-chirped mirrors is calculated such that six bounces compensate for the GDD at 6 mm insertion and 28-cm separation while only four bounces were used in the final laser setup. The desired total cavity GDD is flat and slightly negative.

of about 50 ps, which is somewhat longer compared with 12 ps in [4]. The modulation depth of the fast recovery time is still not large enough to support sub-10-fs pulse generation alone, but the longer absorber recovery time improves the mode-locking buildup time.

C. Dispersion Compensation Using a Combination of DCM's and a Prism Pair

For optimum soliton formation of a sub-10-fs pulse inside the laser, only a very small amount of negative total intracavity dispersion is necessary [22], [42]. This amount |GDD| can be determined from the balance of the chirp due to self-phase modulation with the chirp due to the negative dispersion. The resulting estimate for the dispersion is then given by [43]

$$\text{GDD} = \frac{dT_g}{d\omega} = -2\phi_0 \left(\frac{\tau_{\rm FWHM}}{1.76}\right)^2$$

with

$$\phi_0 = \frac{1}{2}\,\delta |A_0|^2$$

where T_g is the total intracavity group delay within one round-trip, ϕ_0 is the nonlinear phase shift of the soliton pulse per round-trip, $\tau_{\rm FWHM}$ is the pulse duration, δ is the self-phase modulation coefficient and $|A_0|^2$ is the soliton peak power. With a peak power of 11 MW and an estimated self-phase modulation coefficient of about 0.07/MW, we estimate the necessary dispersion to be GDD $= -10$ fs^2. However, the self-phase modulation (SPM) coefficient is not known precisely, because it is inversely proportional to the effective area of the laser mode in the laser crystal and, therefore, can only be estimated from ABCD-matrix calculations of the laser cavity. The strength of SPM also depends on the actual pulsewidth in the laser crystal. Ideally, this small amount of negative total intracavity dispersion, which is approximately zero on the scale shown in Fig. 6, should be constant over a wavelength range as large as possible.

The higher order dispersion of the prism pairs is dominated by the prism spacing which is not significantly changed when we adjust GDD. At a prism spacing of 40 cm the total dispersion that is produced by a double pass through the prism geometry amounts to GDD $= -862$ fs^2 and a third order dispersion of TOD $= d^3\varphi/d\omega^3 = -970$ fs^3 at a center wavelength of 800 nm, assuming zero prism insertion into the beam. We can reduce the negative GDD by moving the prisms into the laser cavity mode: Each additional millimeter of prism insertion produces a positive GDD of 101 fs^2 but only a TOD of 78 fs^3 per cavity round-trip. Therefore, we have sufficient flexibility to overcompensate for the dispersion of the Ti:sapphire crystal, which for a double pass is GDD $= +302$ fs^2 and TOD $= +219$ fs^3 at 800 nm.

The target function to be matched by the designed double-chirped mirrors is given by the inverse of the dispersion due to a round-trip through the crystal and the prism pair. The detailed theory for the DCM-design is presented in [8]. We first assumed that the target dispersion should be accomplished by six bounces on DCM's. For reasons that are discussed in Section III-B, we have later used only two DCM's along with a standard high-reflector instead of three DCM's, in order to obtain a total cavity GDD as flat as possible over a wavelength range as broad as possible. The custom-designed DCM's, that were fabricated by ion-beam sputtering [44], [45], produce a GDD of -50 fs^2 at 800 nm per reflection, which results in a GDD of -400 fs^2 per cavity round-trip for two DCM's. A small variation of the prism insertion controls the second order dispersion of the prism pair and continuously adjusts the total amount of net negative GDD in the cavity.

Although we use a prism separation of 40 cm in our cavity (see Section II-A), the DCM's were originally designed for a prism separation of 28 cm. When we used three DCM's in the cavity, as assumed in the DCM design, the energy content in a spectral spike located around 860 nm became very strong and the pulse width was longer than 7 fs. The shortest pulse and the broadest overall spectrum was generated with two DCM's and one remaining standard high-reflector, as shown in Fig. 1. With only two DCM's, the prism sequence had to be stretched to 40 cm to generate enough negative GDD. Fig. 6 shows the wavelength dependent GDD of a double path through the Ti:sapphire crystal and the prism pair, calculated for 40-cm apex-to-apex separation and different prism insertions into the beam. The increased higher order dispersion for the larger prism separation is obvious compared with the GDD that would be generated by four reflections from the designed DCM's. The maximum of the GDD shifts only slightly, even when the prism insertion is increased considerably. Also the parabolicity of the GDD remains nearly constant. Therefore, we can adjust the GDD by changing the prism insertion without adding much higher order dispersion.

We measured the GDD of the fabricated DCM's using a white-light interferometer [46]. The interferogram is recorded for varying path differences, and the data acquisition is triggered by the interferences of a HeNe laser beam, that travels parallel to the white light. Fast Fourier transform yields the spectral phase as a function of frequency. Double differentiation finally gives the GDD. We averaged 1024 interferograms and finally applied fiftyfold binomial smoothing, which reduced the spectral resolution to about 20 nm. The reproducibility of the GDD between two subsequent measurements is about ± 5 fs^2. We checked the result by comparison with another independent measurement setup [47], that delivered the same GDD within the measurement accuracies. Fig. 7 displays the measured, the desired, and the designed GDD of the DCM. The designed GDD is close to the desired value within ± 10 fs^2, and the observed deviation is due to the finite number of layer pairs. In total, the mirror has 25 TiO_2SiO_2 layer pairs. Limitations in the precision of the layer growth led to deviations of the measured GDD from the designed GDD, see Fig. 7. For short wavelengths, the designed and measured GDD are sufficiently close. However, for wavelengths above 850 nm, the average GDD of the fabricated mirrors is too low. The sensitivity to fabrication errors is larger for the longer wavelength components because they penetrate more deeply into the dielectric multilayer structure and, therefore, are more strongly affected by any errors in the layer growth.

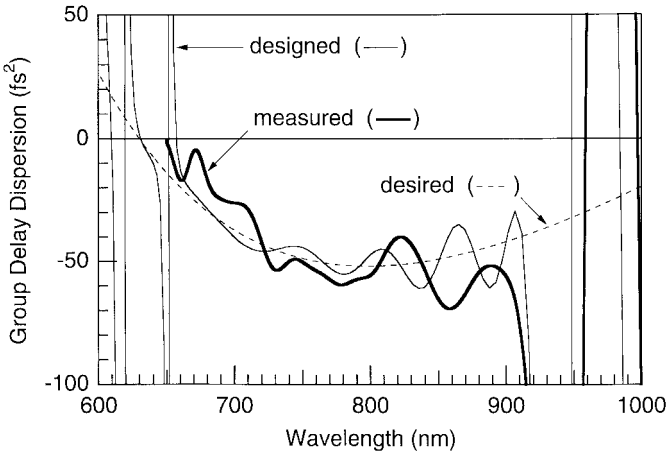

Fig. 7. GDD of the designed mirror structure compared with the desired target function and the measured GDD of the fabricated DCM's. The measurement accuracy is about 5 fs^2.

The measured reflectivity of the DCM is shown in Fig. 8. The top 1% is expanded to demonstrate a high reflectivity greater than 99.8% from almost 650 to 950 nm. The argon ion pump light has to pass through one of the mirrors. Thus, good transmission around 500 nm is very important. Note that the backside of the mirrors has not been antireflection (AR)-coated for the pump light. Anticipated improvements in the fabrication process will most likely also increase the GDD accuracy of our DCM's.

III. Characterization

A. Mode-Locking Buildup Time

To examine the startup behavior of the laser, we put a chopper wheel inside the cavity between the SESAM and the high reflector. The laser is switched on every time a slit in the wheel unblocks the cavity. However, due to the limited frequency of the chopper ($\approx$500 Hz), it takes about 20 μs until the whole beam can pass, leading to a chopper limited slow rise time for the average laser output power

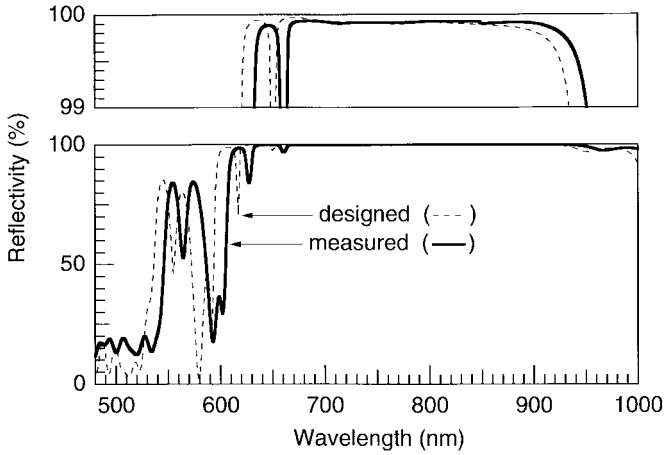

Fig. 8. Measured reflectivity of the fabricated DCM's, compared with the reflectivity expected from the design.

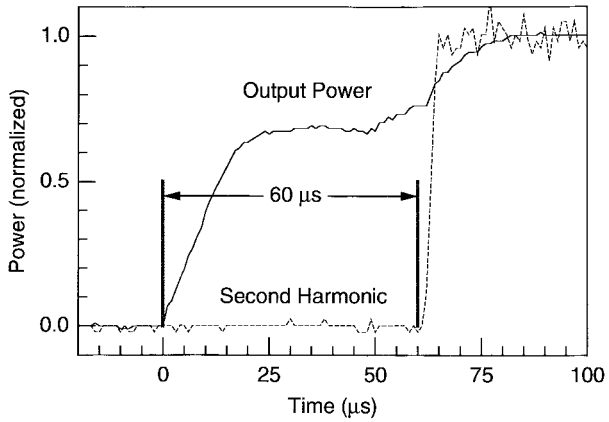

Fig. 9. Mode-locking buildup time, measured with an intracavity chopper. The slow rise of the laser output at the fundamental frequency is due to the limited speed of the chopper wheel. The sharp rise of the frequency doubled output indicates the onset of stable pulsing. The mode-locking buildup time is 60 μs.

(Fig. 9). The laser output is focused onto a KDP crystal to generate frequency doubled light. The intensity of the second harmonic increases sharply as soon as the laser starts emitting short pulses. Therefore, the time delay between the onset of the average power and the second harmonic light determines the mode-locking buildup time. For 6-W pump power, we determined a mode-locking buildup time of only 60 μs in our current setup (Fig. 9) compared to 3 ms in [4].

B. Pulse Spectrum and Interferometric Autocorrelation

First, three DCM's were tested in the cavity, and a prism separation of 28 cm was used, as assumed in the mirror design. With three mirrors, however, it was impossible to mode-lock a spectrum broad enough to support a sub-7-fs pulse, as noted in Section II-C. As we exchanged one DCM with a standard high-reflector, we were also forced to increase the prism separation from 28 to 40 cm, in order to supply for the additional negative GDD that was originally generated from the removed DCM. Fig. 10 shows the measured and calibrated pulse spectrum, obtained with this configuration, together with the dispersion of the different cavity elements,

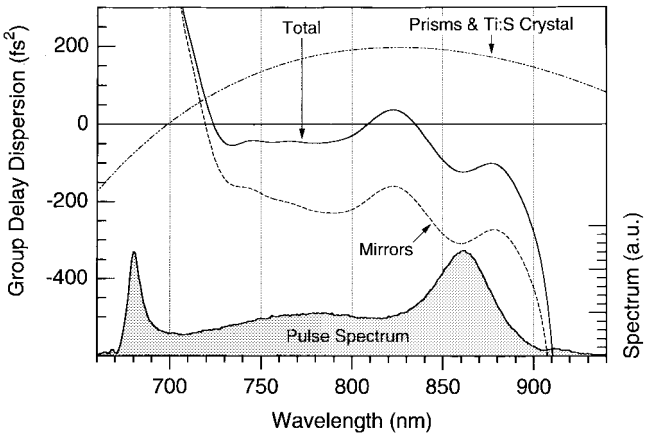

Fig. 10. Calculated group delay dispersion (GDD) of the FS prism pair (40-cm separation), in combination with the material dispersion of Ti:sapphire; measured GDD of two DCM's combined with one high reflector and the output coupler; resulting GDD of all cavity components. The peak of the pulse spectrum at 860 nm coincides with the dip of the net cavity GDD.

and the total cavity dispersion. The spectrum consists of a broad, almost sech^2-shaped main part, and two additional spectral components at 680 nm and around 860 nm. The latter feature also shows a sech^2-shape. This peak was much more pronounced in the spectrum obtained with the initial setup using three DCM's. Apparently it is caused by the deviation from the ideal dispersion around 850 nm and could possibly be eliminated with better mirrors.

The interferometric autocorrelation trace (IAC) has been measured using a KDP crystal, which is wedged from 50 down to about 7 μm, sufficiently thin to exhibit a flat conversion efficiency over the whole laser spectrum. Thin gold coated beamsplitters were used to avoid dispersion in the autocorrelator. The delay was calibrated by simultaneously recording the interference of a collinear HeNe laser beam. Fitting the IAC of a sech^2-pulse to the measured IAC leads to a full width at half maximum (FWHM) of 6.5 fs and a center wavelength of 810 nm [Fig. 11(a)]. The agreement of the fit with the measured IAC is excellent in the center part. Additional wings in the IAC are generated due to the limited contrast ratio of the ultrashort pulse. In contrast, the ideal sech^2-pulse produces an IAC without wings. For lasers with solitary pulse formation, it has been common practice to determine the soliton parameters in this manner. Even with spectra that deviated from an ideal sech^2-shape, the pulse duration has normally been calculated from the autocorrelation assuming an ideal soliton pulse [2], [31], [48].

Another approach estimating the pulse duration follows from the measured power spectrum, assuming in first approximation that the entire spectrum is phase locked. So far, this technique has mainly been used for pulses that were spectrally broadened by nonlinear effects outside the cavity [10]. Assuming a constant phase, we Fourier transform the square root of the measured power spectrum (Fig. 10), which yields the complex electric field of the pulse. The intensity envelope of this calculated field has a FWHM of 6.7 fs, which is in reasonable agreement with the value obtained from the sech^2-fit. While an ideal 6.5-fs sech^2-pulse fits slightly better to the

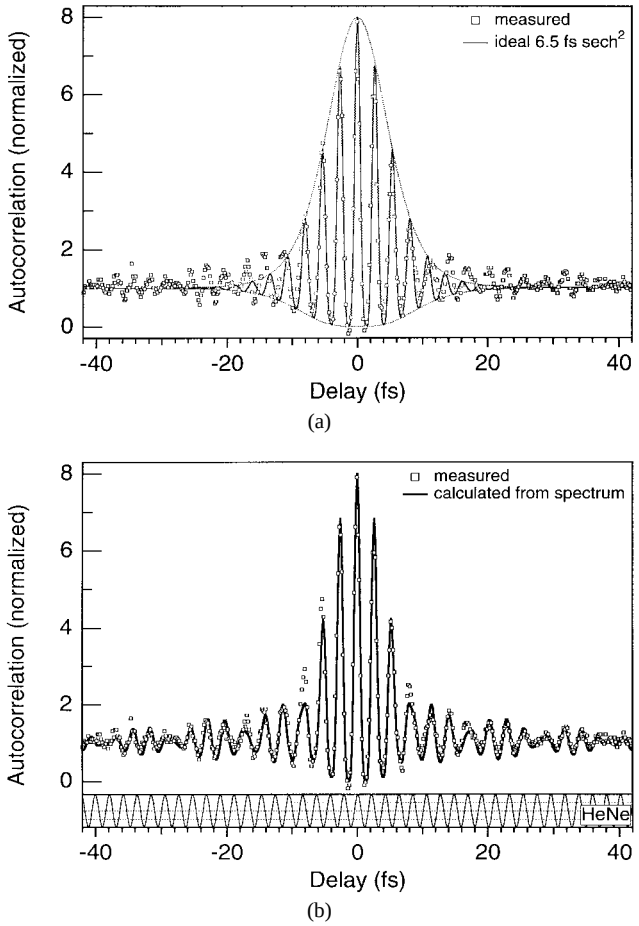

Fig. 11. (a) IAC. The squares denote the IAC, measured with a thin KDP crystal. The IAC of an ideal soliton of 6.5-fs duration centered at 810 nm is shown for comparison. (b) The measured IAC, and the IAC computed from the pulse which is calculated from the measured spectrum, assuming zero phase. The delay is calibrated with the interference of a HeNe laser beam.

center part of the measured IAC, the IAC derived from the calculated field gives a much better fit to the wings [Fig. 11(a), (b)]. Thus, the assumption of a constant phase for the whole pulse spectrum seems to be surprisingly accurate. The undesired narrow spectral components at 680 nm and around 860 nm (Fig. 10) correspond to longer subpulses that do not change the FWHM of the pulse but add to the pulse pedestal.

IV. Discussion

A. Mode-Locking Buildup Time

To date, no sub-50-fs KLM laser has been demonstrated without the use of additional starting mechanisms. Even for pulses longer than 50 fs, typical mode-locking buildup times of self-starting KLM pulses amount to several milliseconds [49], [50]. This is due to the fact that the Kerr nonlinearity is strong only for the high peak intensities of ultrashort pulses. The low intensity of CW light is much too weak to initiate mode-locking via the Kerr effect. Additional starting mechanisms such as an external shaker [3], [51] or a saturable absorber are necessary to initiate KLM for shorter pulses.

The mode-locking buildup time in a laser started by a saturable absorber is approximately proportional to the saturation intensity of the absorber divided by its modulation depth [52],

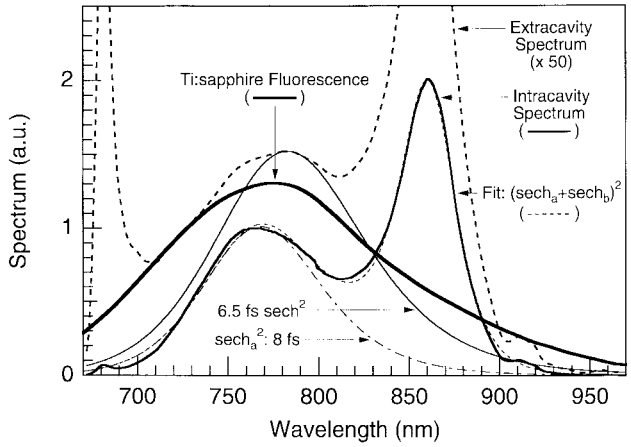

Fig. 12. Extracavity and intracavity spectrum. The intracavity spectrum is calculated by dividing the measured pulse spectrum by the transmission of the output coupler, see Fig. 13. The intracavity spectrum can be fitted to the sum of an ideal 8-fs sech-pulse centered at 770 nm and a 21-fs pulse centered at 860 nm. The spectrum of an ideal 6.5-fs sech^2-soliton and the fluorescence of Ti:sapphire are shown for comparison with the measured pulse spectrum.

[53]. Both parameters determine the slope of the saturable absorption as a function of incident energy. The growth rate of neighboring modes is proportional to this slope. Our current SESAM shows a modulation depth increased by a factor of 3.5 and a carrier saturation intensity decreased by a factor of 14 compared to the one used in [4], see Section II-C (the saturation intensity is the saturation fluence divided by the absorber recovery time). This explains the improvement by a factor of 50 in the mode-locking buildup time in comparison with the results achieved earlier.

B. Pulse Spectrum and Duration

The spectrum of the extracavity laser pulse covers almost the whole fluorescence bandwidth of the gain material (Fig. 12). To understand the origin of the spike at 680 nm, we must look at the influence of the output coupler on the emitted spectrum. Division of the output spectrum by the transmission of the output coupler (Fig. 13) results in the intracavity spectrum shown in Fig. 12. Fig. 12 clearly demonstrates that the external pulse spectrum is actually much broader than the intracavity spectrum. From the Fourier transform of the intracavity spectrum, we obtain an intracavity pulse duration of slightly less than 9 fs. The enhanced output coupling at short wavelengths lifts the spectral components in that wavelength range considerably. This leads to a much broader spectrum and, therefore, to a shorter pulse. The spectral spike located at 680 nm is generated by the substantially higher output coupling at wavelengths below 690 nm close to the cutoff of the output coupler (Figs. 10 and 13). The spike is even further enhanced by phase matching of the solitary pulse and the continuum that also occurs close to the cutoff limit of the output coupler [54].

The net average GDD at short wavelengths supports an intracavity soliton-like pulse centered at 770 nm, which contains roughly 60% of the total pulse energy in the cavity. Its bandwidth of about 40 THz corresponds to an ideal soliton of sub-8-fs duration. The narrow sech^2-shaped spectral

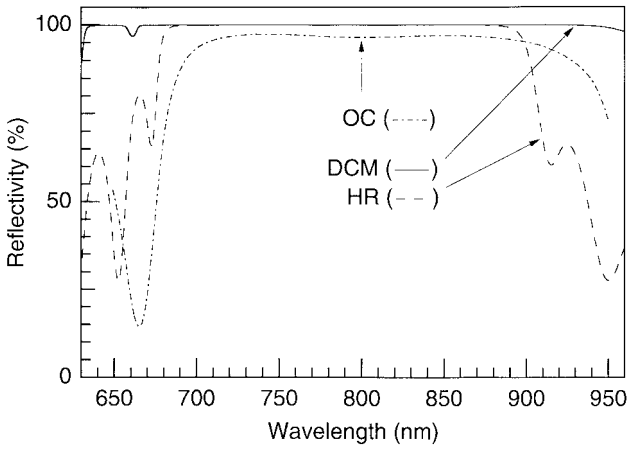

Fig. 13. Measured reflectivities of the cavity mirrors, revealing the broad bandwidth of the DCM compared to the standard dielectric HR and the 3% OC. The OC shows a slightly increased transmission around 800 nm and a high transmission of ≈85% at 670 nm.

feature around 860 nm is caused by the long-wavelength GDD error of the fabricated DCM's (Figs. 7 and 10). This error results in a second soliton-like pulse with 21-fs duration, that contains the remaining 40% of the pulse energy. We want to point out that cutting off the spectrum of the ideal 8-fs sech^2-pulse at the margins of our observed spectrum considerably increases the FWHM of the pulse to 10 fs. This effect is less severe for the spectrum of the 21-fs pulse. As noted above, the IAC computed from the spectrum, assuming zero phase, fits the measured IAC remarkably well [Fig. 11(b)]. This indicates that the two pulses are phase locked together, forming a single ultrashort pulse with some pedestals. Proving this more directly is only possible if the phase over the total pulse spectrum is investigated in more detail, using, for example, frequency resolved optical gating [55]. Noncollinear autocorrelation techniques, however, suffer from an inherent smearing-out of the derived pulse shape [56]. The collinear technique of spectral shearing interferometry provides a promising alternative. It requires no moving parts, it has a rapid noniterative pulse retrieval algorithm, and it could thus be used for a real-time observation of the pulse shape [57].

The broad central dip of the output coupler reflectivity considerably lifts the central part of the spectrum as well (compare Figs. 12 and 13). While the sech^2-like part of the extracavity spectrum readily corresponds to a 7-fs laser pulse, the two additional spectral peaks decrease the FWHM of the pulse even further due to constructive interference at the peak of the ultrashort pulse and destructive interference at the half width. Unfortunately, the spectrally narrow spikes also lead to an undesirable background. This would limit the time resolution of an ultrafast measurement. Further improvements of our DCM's should eliminate these problems in the future. However, the described pulses have the shortest FWHM that has been demonstrated directly from a laser to date.

V. Conclusion

We have generated self-starting KLM pulses as short as 6.5 fs from a Ti:sapphire laser with an average output power of 200 mW and a pulse repetition rate of 86 MHz. Two key components were responsible for this result. First, a broadband SESAM reliably started the mode-locking process and produced a mode-locking buildup time of only 60 μs. Second, controlled dispersion over the full bandwidth was obtained with a combination of DCM's and a fused quartz prism pair. We demonstrated that a properly designed output coupler can lead to shorter extracavity pulses when its transmission shapes the intracavity spectrum accordingly. Improvements in the fabrication of the DCM's should lead to a cleaner spectrum and possibly even shorter pulses. However, new approaches will be necessary in the SESAM design in order to mode-lock even broader pulse spectra. The dispersion compensation with DCM's and the very efficient starting mechanism will be the basis for a compact and reliable sub-10-fs laser technology in the near future.

References

[1] D. E. Spence, P. N. Kean, W. Sibbett, "60-fsec pulse generation from a self-mode-locked Ti:sapphire laser," *Opt. Lett.*, vol. 16, pp. 42–44, 1991.
[2] J. Zhou, G. Taft, C.-P. Huang, M. M. Murnane, H. C. Kapteyn, and I. P. Christov, "Pulse evolution in a broad-bandwidth Ti:sapphire laser," *Optics Lett.*, vol. 19, pp. 1149–51, 1994.
[3] L. Xu, C. Spielmann, F. Krausz, and R. Szipöcs, "Ultrabroadband ring oscillator for sub-10-fs pulse generation," *Opt. Lett.*, vol. 21, pp. 1259–1261, 1996.
[4] I. D. Jung, F. X. Kärtner, N. Matuschek, D. H. Sutter, F. Morier-Genoud, G. Zhang, U. Keller, V. Scheuer, M. Tilsch, and T. Tschudi, "Self-starting 6.5 pulses fs from a Ti:sapphire laser," *Opt. Lett.*, vol. 22, pp. 1009–1011, 1997.
[5] R. Fluck, I. D. Jung, G. Zhang, F. X. Kärtner, and U. Keller, "Broadband saturable absorber for 10 fs pulse generation," *Opt. Lett.*, vol. 21, pp. 743–745, 1996.
[6] I. D. Jung, F. X. Kärtner, N. Matuschek, D. H. Sutter, F. Morier-Genoud, Z. Shi, V. Scheuer, M. Tilsch, T. Tschudi, and U. Keller, "Semiconductor saturable absorber mirrors supporting sub-10 fs pulses," *Appl. Phys. B* (special issue on ultrashort pulse generation), vol. 65, pp. 137–150, 1997.
[7] F. X. Kärtner, N. Matuschek, T. Schibli, U. Keller, H. A. Haus, C. Heine, R. Morf, V. Scheuer, M. Tilsch, and T. Tschudi, "Design and fabrication of double-chirped mirrors," *Opt. Lett.*, vol. 22, pp. 831–833, 1997.
[8] N. Matuschek, F. X. Kärtner, and U. Keller, "Theory of Double-Chirped Mirrors," this issue, pp. 197–208.
[9] A. Baltuska, Z. Wei, M. S. Pshenichnikov, and D. A. Wiersma, "Optical pulse compression to 5 fs at 1 MHz repetition rate," *Opt. Lett.*, vol. 22, pp. 102–104, 1997.
[10] A. Baltuska, Z. Wei, M. S. Pshenichnikov, D. A. Wiersma, and R. Szipöcs, "All-solid-state cavity dumped sub-5-fs laser," *Appl. Phys. B*, vol. 65, pp. 175–188, 1997.
[11] M. Nisoli, S. De Silvestri, O. Svelto, R. Szipöcs, K. Ferenz, C. Spielmann, S. Sartania, and F. Krausz, "Compression of high energy laser pulses below 5 fs," *Opt. Lett.*, vol. 22, pp. 522–524, 1997.
[12] M. Nisoli, S. Stagira, S. D. Silvestri, O. Svelto, S. Sartania, Z. Cheng, M. Lenzner, C. Spielmann, and F. Krausz, "A novel-high energy pulse compression system: generation of multigigawatt sub-5-fs pulses," *Appl. Phys. B*, vol. 65, pp. 189–196, 1997.
[13] S. Sartania, Z. Cheng, M. Lenzner, G. Tempea, C. Spielmann, F. Krausz, K. Ferencz, "Generation of 0.1-TW 5-fs optical pulses at a 1-kHz repetition rate," *Opt. Lett.*, vol. 22, pp. 1562–1564, 1997.
[14] I. P. Christov, J. Zhou, J. Peatross, A. Rundquist, M. M. Murnane, and H. C. Kapteyn, "Nonadiabatic effects in high-harmonic generation with ultrashort pulses," *Phys. Rev. Lett.*, vol. 77, p. 1743, 1996.
[15] J. Zhou, J. Peatross, M. M. Murnane, and H. C. Kapteyn, "Enhanced high-harmonic generation using 25 fs laser pulses," *Phys. Rev. Lett.*, vol. 76, p. 752, 1996.
[16] C. Spielmann, N. H. Burnett, S. Sartania, R. Koppitsch, M. Schnurer; C. Kan; M. Lenzner, P. Wobrauschek, and F. Krausz, "Generation of coherent X-rays in the water window using 5-femtosecond laser pulses," *Science*, vol. 278, pp. 661–664, 1997.
[17] Z. Chang, A. Rundquist, H. Wang, H. Kapteyn, and M. Murnane, "Generation of coherent soft-x-rays below 2.7 nm using high harmonic generation," *Phys. Rev. Lett.*, vol. 79, 2967–2970, 1997.

[18] M. C. Nuss, "Information processing with short optical pulses," in *Proc. Conf. LEOS'96*, 1996, vol. 2, pp. 338–339.
[19] A. M. Weiner, C.-C. Chang, and H. P. Sardesai, "Femtosecond optical code-division multiple-access," presented at the OSA Spring Top. Meet. Ultrafast Electronics and Optoelectronics 1997.
[20] B. Bouma, G. J. Tearney, S. A. Boppart, M. R. Hee, M. E. Brezinski, and J. G. Fujimoto, "High-resolution optical coherence tomograhic imaging using a mode-locked Ti:Al_2O_3 laser source," *Opt. Lett.*, vol. 20, pp. 1486–1488, 1995.
[21] D. P. DiVincenco, "Quantum computing," *Science*, vol. 270, pp. 255–261, 1995.
[22] C. Spielmann, P. F. Curley, T. Brabec, and F. Krausz, "Ultrabroadband femtosecond lasers," *IEEE J. Quantum Electron.*, vol. 30, pp. 1100–1114, 1994.
[23] F. X. Kärtner, and U. Keller, "Stabilization of soliton-like pulses with a slow saturable absorber," *Opt. Lett.*, vol. 20, pp. 16–18, 1995.
[24] I. D. Jung, F. X. Kärtner, L. R. Brovelli, M. Kamp, and U. Keller, "Experimental verification of soliton modelocking using only a slow saturable absorber," *Opt. Lett.*, vol. 20, pp. 1892–1894, 1995.
[25] F. X. Kärtner, I. D. Jung, and U. Keller, "Soliton Modelocking with Saturable Absorbers," *IEEE J. Select. Topics Quantum Electron.*, vol. 2, pp. 540–556, 1996.
[26] R. L. Fork, O. E. Martinez, and J. P. Gordon, "Negative dispersion using pairs of prisms," *Opt. Lett.*, vol. 9, pp. 150–152, 1984.
[27] M. T. Asaki, C.-P. Huang, D. Garvey, J. Zhou, H. C. Kapteyn, and M. N. Murnane, "Generation of 11-fs pulses from a self-mode-locked Ti:sapphire laser," *Opt. Lett.*, vol. 18, pp. 977–979, 1993.
[28] C.-P. Huang, M. T. Asaki, S. Backus, M. M. Murnane, H. C. Kapteyn, and H. Nathel, "17-fs pulses from a self-mode-locked Ti:sapphire laser," *Opt. Lett.*, vol. 17, pp. 1289–1291, 1992.
[29] I. P. Christov, V. D. Stoev, M. M. Murnane, and H. C. Kapteyn, "Sub-10-fs operation of Kerr-lens mode-locked lasers," *Opt. Lett.*, vol. 21, pp. 1493–1495, 1996.
[30] I. P. Christov, M. M. Murnane, H. C. Kapteyn, J. Zhou, and C. P. Huang, "Fourth-order dispersion-limited solitary pulses," *Opt. Lett.*, vol. 19, pp. 1465–1467, 1994.
[31] L. Xu, G. Tempea, A. Poppe, M. Lenzner, C. Spielmann, F. Krausz, A. Stingl, and K. Ferencz, "High-power sub-10-fs Ti:sapphire oscillators," *Appl. Phys. B*, vol. 65, pp. 151–159, 1997.
[32] R. Szipöcs, K. Ferencz, C. Spielmann, and F. Krausz, "Chirped multilayer coatings for broadband dispersion control in femtosecond lasers," *Opt. Lett.*, vol. 19, pp. 201–203, 1994.
[33] R. Szipöcs, A. Stingl, C. Spielmann, and F. Krausz, "Chirped dielectric mirrors for dispersion control in femtosecond laser systems," F. W. Wise, C. P. J. Barty, Eds., in *Proc. SPIE 1995, Generation, Amplification, and Measurement of Ultrashort Laser Pulses II*, pp. 11–22.
[34] ———, "Pushing the limits of femtosecond technology: Chirped dielectric mirrors" *Opt. Photon. News*, pp. 16–22, June 1995.
[35] P. W. Smith, Y. Silberberg, and D. A. B. Miller, "Modelocking of semiconductor diode lasers using saturable excitonic nonlinearities," *J. Opt. Soc. Amer. B*, vol. 2, pp. 1228–1236, 1985.
[36] P. J. Delfyett, L. T. Florez, N. Stoffel, T. Gmitter, N. C. Andreadakis, Y. Silberberg, J. P. Heritage, and G. A. Alphonse, "High-power ultrafast laser diodes," *IEEE J. Quantum Electron.*, vol. 28, pp. 2203–2219, 1992.
[37] U. Keller, D. A. B. Miller, G. D. Boyd, T. H. Chiu, J. F. Ferguson, and M. T. Asom, "Solid-state low-loss intracavity saturable absorber for Nd:YLF lasers: An antiresonant semiconductor Fabry–Perot saturable absorber," *Opt. Lett.*, vol. 17, pp. 505–507, 1992.
[38] U. Keller, K. J. Weingarten, F. X. Kärtner, D. Kopf, B. Braun, I. D. Jung, R. Fluck, C. Hönninger, N. Matuschek, and J. Aus der Au, "Semiconductor saturable absorber mirros (SESAM's) for femtosecond to nanosecond pulse generation in solid-state lasers," *IEEE J. Select. Topics Quantum Electron.*, vol. 2, pp. 435–453, 1996.
[39] U. Keller, "Semiconductor nonlinearities for solid-state laser modelocking and Q-switching," in *Nonlinear Optics in Semiconductors*, A. Kost, E. Garmire, Eds. Boston, MA: Academic, 1998.
[40] W. van der Osten, O. Madelung, and U. Rössler, *Numerical Data and Functional Relationships in Science and Technology*, O. Madelung, Ed. New York, Springer, Landold-Börnstein, 1987, vol. III/22a.
[41] Y. H. Lee, A. Chavez-Pirson, S. W. Koch, H. M. Gibbs, S. H. Park, J. Morhange, A. Jeffery, N. Peyghambarian, L. Banyai, A. C. Gossard, and W. Wiegmann, "Room temperature optical nonlinearities in GaAs," *Phys. Rev. Lett.*, vol. 57, p. 2446, 1986.
[42] C. Spielmann, F. Krausz, T. Brabec, E. Wintner, and A. J. Schmidt, "Femtosecond passive modelocking of a solid-state laser by dispersively balanced nonlinear interferometer," *Appl. Phys. Lett.*, vol. 58, pp. 2470–2472, 1991.
[43] H. A. Haus, J. G. Fujimoto, and E. P. Ippen, "Structures for additive pulse modelocking," *Opt. Soc. Amer. B*, vol. 8, pp. 2068–2076, 1991.
[44] V. Scheuer, M. Tilsch, and T. Tschudi, "Reduction of absorption losses in ion beam sputter deposition of optical coatings for the visible and near infrared," in *Proc. Conf. SPIE*, 1994, vol. 2253, pp. 445–454.
[45] M. Tilsch, V. Scheuer, J. Staub, and T. Tschudi, "Direct optical monitoring instrument with a double detection system for the control of multilayer systems from the visible to the near infrared," in *Proc. Conf. SPIE*, 1994, vol. 2253, pp. 414–422.
[46] K. Naganuma, K. Mogi, and H. Yamada, "Group-delay measurement using the Fourier transform of an interferometric cross correlation generated by white light," *Opt. Lett.*, vol. 15, pp. 393–395, 1990.
[47] A. P. Kovacs, K. Osvay, Z. Bor, and R. Szipocs, "Group-delay measurement on laser mirrors by spectrally resolved white-light interferometry," *Opt. Lett.*, vol. 20, p. 788, 1995.
[48] R. L. Fork, C. H. B. Cruz, P. C. Becker, and C. V. Shank, "Compression of optical pulses to six femtoseconds by using cubic phase compensation," *Opt. Lett.*, vol. 12, pp. 483–485, 1987.
[49] G. Cerullo, S. De Silvestri, and V. Magni, "Self-starting Kerr lens modelocking of a Ti:sapphire laser," *Opt. Lett.*, vol. 19, pp. 1040–1042, 1994.
[50] G. Cerullo, S. De Silvestri, V. Magni, and L. Pallaro, "Resonators for Kerr-lens mode-locked femtosecond Ti:sapphire lasers," *Opt. Lett.*, vol. 19, pp. 807–809, 1994.
[51] A. Kasper and K. J. Witte, "10-fs pulse generation from a uni-directional Kerr-lens mode-locked Ti:sapphire ring laser," *Opt. Lett.*, vol. 21, p. 360, 1996.
[52] H. A. Haus, "Parameter ranges for CW passive modelocking," *IEEE J. Quantum Electron.*, vol. QE-12, pp. 169–176, 1976.
[53] F. X. Kärtner, L. R. Brovelli, D. Kopf, M. Kamp, I. Calasso, and U. Keller, "Control of solid-state laser dynamics by semiconductor devices," *Opt. Eng.*, vol. 34, pp. 2024–2036, 1995.
[54] P. F. Curley, C. Spielmann, T. Brabec, F. Krausz, E. Wintner, and A. J. Schmidt, "Operation of a femtosecond Ti:sapphire solitary laser in the vicinity of zero group-delay dispersion," *Opt. Lett.*, vol. 18, pp. 54–56, 1993.
[55] R. Trebino, K. W. DeLong, D. N. Fittinghoff, J. Sweetser, M. A. Krumbügel, and B. Richman, "Measuring ultrashort laser pulses in the time-frequency domain using frequency-resolved optical gating," *Rev. Sci. Instrum.*, vol. 68, pp. 1–19, 1997.
[56] G. Taft, A. Rundquist, M. M. Murnane, I. P. Christov, H. C. Kapteyn, K. W. DeLong, D. N. Fittinghoff, M. A. Krumbügel, J. N. Sweetser, and R. Trebino, "Measurement of 10-fs laser pulses," *IEEE J. Select. Topics Quantum Electron.*, vol. 2, pp. 575–585, 1996.
[57] C. Iaconis and I. A. Walmsley, "Spectral shearing interferometry for measuring the amplitude and phase of ultrashort optical pulses," presented at the Conf. Ultrafast Optics, Monterey, CA, Aug. 1–7, 1997, paper MA–4.

Dirk H. Sutter received the diploma degree in ultrafast characterization of high-speed laser diodes from the Fraunhofer-Insitute for Applied Physics, Albert-Ludwigs-University, Freiburg, Germany, in 1996 and is working towards the Ph.D. degree at the Institute of Quantum Electronics, ETH Zurich.

His research interest is focused on ultrashort pulse generation, measurement, and application.

Isabella D. Jung was born in Munich, Germany in 1968. She received the diploma degree in physics from the Ludwig-Maximilians-University, Munich, Germany, in 1993, and the Ph.D. degree in ultrafast pulse generation from the Institute of Quantum Electronics, ETH, Zurich, Switzerland, in 1997.

She is now a Project Manager for externally stabilized semiconductor laser diodes at Uniphase Laser Enterprises, Zurich, Switzerland.

Franz X. Kartner, for photograph and biography, see this issue, p. 168.

Nicolai Matuschek was born in Biberach an der Riß, Germany, in 1968. He received the diploma degree in physics from the University Ulm, Ulm, Germany, in 1995 and is working towards the Ph.D. degree at the Institute of Quantum Electronics, Swiss Federal Institute of Technology (ETH) Zurich, Switzerland.

After finishing his diploma degree in the field of theoretical polymer physics, he changed his research interests to laser physics, where he is currently focused on the theory of mode-locked solid-state lasers.

François Morier-Genoud was born in Geneva, Switzerland, in 1959. He received the diploma degree in microtechnical engineering from the Swiss Technical University, Yverdon, Switzerland, in 1981.

From 1986 to 1995, he worked in the field of III–V semiconductor compunds by developing crystal growth techniques for optoelectronic devices (lasers and modulators) at the Swiss Federal Institute of Technology (EPFL), Lausanne, Switzerland. Since 1995, he is with the Institute of Quantum Electronics (ETHZ), Zurich, Switzerland. His research topics are focused on growth and characterization of III–V semiconductor heterostructures for ultrafast lasers systems.

V. Scheuer, photograph and biography not available at the time of publication.

M. Tilsch, photograph and biography not available at the time of publication.

T. Tschudi, photograph and biography not available at the time of publication.

Ursula Keller (M'89), for photograph and biography, see this issue, p. 168.